

DeepStream: Prototyping Deep Joint Source-Channel Coding for Real-Time Multimedia Transmissions

Kaiyi Chi, Yinghui He, Qianqian Yang, Member, IEEE, Zhiping Jiang, Yuanchao Shu, Senior Member, IEEE, Zhiqin Wang, Jun Luo, Fellow, IEEE, and Jiming Chen, Fellow, IEEE

Abstract—Deep learning-based joint source-channel coding (DeepJSCC) has emerged as a promising technique in 6G for enhancing the efficiency and reliability of data transmission across diverse modalities, particularly in low signal-to-noise ratio (SNR) environments. This advantage is realized by leveraging powerful neural networks to learn an optimal end-to-end mapping from the source data directly to the transmit symbol sequence, eliminating the need for separate source coding, channel coding, and modulation. Although numerous efforts have been made towards efficient DeepJSCC, they have largely stayed at numerical simulations that can be far from practice, leaving the real-world viability of DeepJSCC largely unverified. To this end, we prototype DeepStream upon orthogonal frequency division multiplexing (OFDM) technology to offer efficient and robust DeepJSCC for multimedia transmission. In conforming to OFDM, we develop both a feature-to-symbol mapping method and a cross-subcarrier precoding method to improve the subcarrier independence and reduce peak-to-average power ratio. To reduce system complexity and enable flexibility in accommodating varying quality of service requirements, we further propose a progressive coding strategy that adjusts the compression ratio based on latency with minimal performance loss. We implement DeepStream for real-time image transmission and video streaming using software-defined radio. Extensive evaluations verify that DeepStream outperforms both the standard scheme and the direct deployment scheme. Particularly, at an SNR of 10 dB, DeepStream achieves a PSNR of 35 dB for image transmission and an MS-SSIM of 20 dB for video streaming, whereas the standard scheme fails to recover meaningful information.

Index Terms—Joint source-channel coding, semantic communications, prototyping, multimedia transmissions.

I. Introduction

The upcoming sixth-generation (6G) wireless networks are envisioned to support data-intensive applications with extreme reliability and ubiquitous connectivity [1]. In specific use cases such as augmented reality (AR) and

unmanned aerial vehicles (UAVs), the volume of data to be transmitted is substantial, posing significant challenges for conventional communication systems [2], [3]. For example, remote UAV control systems that rely on high-definition video streaming require highly efficient and robust transmission techniques [4]. As a result, the demand for effective transmission of multimedia data across various modalities has increased exponentially. Recent advances in deep learning (DL) have enabled the development of DL-based codecs and communication systems that leverage the powerful feature extraction and representation capabilities of neural networks. These systems have demonstrated strong potential in significantly improving transmission efficiency, particularly under challenging wireless conditions [5], [6].

However, most existing works rely on a critical assumption that the encoded content is transmitted reliably over the wireless channel [7], [8]. In practice, wireless channels are prone to disturbances, leading to errors in the transmitted data, especially under low signal-to-noise ratio (SNR) conditions, as shown in Fig. 1. In such scenarios, conventional approaches like forward error correction (FEC) [9] and retransmission mechanisms often fail to meet stringent latency requirements. This limitation underscores the need for more efficient and noise-resilient transmission schemes tailored to the challenges of wireless environments. Deep joint source-channel coding (DeepJSCC) has emerged as a promising technique to overcome these challenges [10]–[14], and is widely regarded as a key enabler for enhancing both transmission efficiency and robustness in next-generation wireless systems. Unlike the conventional separation-based approach, as depicted in Fig. 1, a DeepJSCC system trains the entire “encoding-decoding” process end-to-end, with the wireless channel incorporated as an integral part of the model. This holistic approach not only improves transmission efficiency but also enhances robustness against channel-induced noise.

To fulfill this goal, numerous DeepJSCC schemes have been proposed to enable efficient and robust transmission of images [15]–[19], speech [20], [21], and video [22], [23] over wireless channels. While these schemes have demonstrated superior performance compared to traditional codecs in simulations, usually considering additive white Gaussian noise (AWGN) channel, the scenarios explored in these studies remain largely idealized. Some efforts

Kaiyi Chi, Qianqian Yang, Yuanchao Shu, and Jiming Chen are with the State Key Laboratory of Industrial Control Technology, Zhejiang University, Hangzhou 310027, China (e-mail: {chikaiyi17, qianqianyang20, ycshu, cjm}@zju.edu.cn).

Yinghui He and Jun Luo are with the College of Computing and Data Science, Nanyang Technological University, Singapore 639798 (email: {yinghui.he, junluo}@ntu.edu.sg).

Zhiping Jiang is with the School of Computer Science and Technology, Xidian University, Xi'an 710126, China (e-mail: zpj@xidian.edu.cn).

Zhiqin Wang is with the School of Information and Communication Engineering, Beijing University of Posts and Telecommunications, Beijing 100876, China, and also with China Academy of Information and Communications Technology, Beijing 100191, China (e-mail: zhiqin.wang@caict.ac.cn).

Building an OFDM-based DeepJSCC system presents several key challenges, as illustrated in Fig. 1. First, unlike traditional coding schemes, DL-based JSCC encoders generate highly correlated feature sequences. This violates a fundamental assumption of OFDM, namely that symbols mapped to different subcarriers should be statistically independent [30], [31], which can significantly degrade performance. Second, the strong correlation among these generated symbols also leads to a high peak-to-average power ratio (PAPR) [32]. More critically, the continuous-valued and unconstrained nature of the semantic feature further exacerbates this issue, leading to nonlinear distortion. Third, most existing encoders and decoders are trained with a fixed compression ratio [12], [17], while real-world applications require adaptive compression to meet varying latency and quality of service (QoS) constraints. Achieving adaptability in these systems typically requires multiple encoder-decoder pairs, which impose significant computational and storage overhead. Finally, existing DeepJSCC systems for video transmission predominantly focus on file transfer, where the entire video is transmitted before playback. In contrast, real-time streaming, critical for practical deployment, remains largely underexplored, even in simulation studies.

In response to these challenges, we propose DeepStream, which, to the best of our knowledge, is the first real-time noise-resilient DeepJSCC prototype designed for efficient and robust multimedia transmission. DeepStream addresses the aforementioned issues through several key innovations. To address the first and second challenges, we develop a mapping method from the task-relevant features to the data symbol and a cross-subcarrier pre-

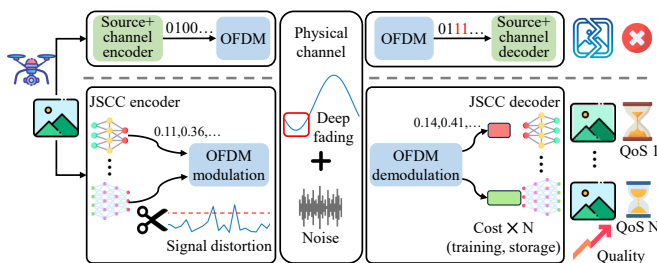


Fig. 1: Comparison between conventional (top) and DeepJSCC (bottom), along with key challenges in prototyping DeepJSCC.

coding method to mitigate inter-symbol correlation across subcarriers and reduce PAPR, thereby enhancing compatibility with OFDM. Furthermore, we propose a progressive coding strategy that prioritizes the transmission of important features while a tailored training mechanism is incorporated to ensure feature importance decreases gradually. Finally, we implement DeepStream on a software-defined radio (SDR) platform, supporting real-time image transmission and video streaming, and further conduct extensive experiments to evaluate DeepStream’s performance. In summary, our main contributions are as follows:

- We prototype DeepStream, the first real-time noise-resilient DeepJSCC system for efficient and robust multimedia transmission.
- We design a feature-to-symbol mapping method and a cross-subcarrier precoding method to ensure symbol decorrelation and reduce PAPR, enhancing the compatibility of DeepJSCC with OFDM.
- We develop a progressive coding strategy that transmits the important features first, enabling adaptive compression to meet varying transmission latency and QoS constraints.
- We implement DeepStream on an SDR platform for real-time image transmission and video streaming and validate its performance through extensive experiments.

The remainder of this paper is organized as follows. Section II briefly discusses related works in the field. Section III provides the background and motivation behind DeepStream. Section IV details the system design of DeepStream, including its key components. Sections V and VI present the experiment setup and performance evaluation results, respectively. Section VII discusses the future work and Section VIII concludes the paper.

Our work is closely related to the loss-resilient source coding [33]–[36] that aims to mitigate packet loss during transmission through innovative DL-based source encoder and decoder designs. One approach involves incorporating packet loss simulations during training to enhance the robustness of the encoder and decoder. For image transmission, Starfish [33] introduces a resilient image compression method that enhances robustness by randomly dropping features during training to simulate packet loss. For video transmission, GRACE [35] improves loss resilience by jointly training neural encoders and decoders under simulated packet loss conditions. Another approach is to leverage generative neural networks on the decoder to reconstruct missing image data [36]. Despite these advancements, their improvements remain confined to source coding. Under low-SNR conditions, severe packet loss leads to performance degradation that is difficult to compensate for.

To overcome this limitation, DL-based JSCC has been explored as an effective and robust transmission solution [12], [17], [22]–[24], [37]–[39]. Bourtsoulatz et al. [12] propose DeepJSCC, a CNN-based JSCC scheme optimized for image transmission. The results demonstrate that

DeepJSCC achieves robust performance under low SNR conditions. Xu et al. [17] extend DeepJSCC using an attention mechanism, incorporating SNR as input to enhance both encoding and decoding processes. Wang et al. [22] further adapt DeepJSCC to video transmission, demonstrating superior performance in low-SNR conditions. To enhance compatibility with existing digital communication systems, Tung et al. [39] propose DeepJSCC-Q, which maps features to the nearest constellation points. However, these studies primarily focus on AWGN channels, which are different from real-world wireless environments. To address the issue, Yang et al. [24] extend JSCC to multipath channels, while Wu et al. [25] apply it to multiple-input multiple-output systems. relay channel network. Liu et al. [40] propose an SDR-based image transmission framework, but did not consider the effect of the multipath fading channel. In parallel, growing research efforts have explored resource allocation and system management strategies tailored for DeepJSCC systems to further enhance their deployment efficiency [26], [41]–[43].

III. Background and Motivation

In this section, we first introduce the fundamentals of DeepJSCC and OFDM, followed by an analysis of why directly integrating them leads to poor performance in practical deployments.

A. DeepJSCC and OFDM

Unlike traditional source and channel coding, DeepJSCC leverages powerful neural networks to perform end-to-end source and channel coding jointly. Fig. 2(a) illustrates a representative DeepJSCC system, consisting of a JSCC encoder and a decoder. The encoder extracts task-relevant features \mathbf{s} from source content (image or video). A popular choice for the JSCC encoder is a convolutional neural network architecture [10], where the extracted feature has a size of $H \times W \times C$, where H , W , and C denote the height, the width, and the number of feature channels, respectively. The JSCC decoder leverages the error correction capabilities of neural networks to reconstruct the content. The encoder and decoder are jointly trained following an end-to-end learning manner, where the channel is incorporated into training to enhance noise resilience. As shown in Fig. 3(a), DeepJSCC achieves a high peak signal-to-noise ratio (PSNR) even at low SNR for image transmission, effectively mitigating the cliff effect observed in the conventional scheme with FEC [12].

To facilitate practical deployment, integrating DeepJSCC with OFDM is essential, as OFDM has become the foundation of mainstream systems such as Wi-Fi and 4G/5G. Fig. 2(b) illustrates the OFDM transmission process, where K denotes the number of subcarriers. The modulation process includes inverse discrete Fourier transform (IDFT) and cyclic prefix (CP) insertion. For an OFDM symbol consisting of K^d data symbols $\mathbf{x}^d \in \mathbb{C}^{K^d}$ and $(K - K^d)$ data pilot (used for phase tracking and

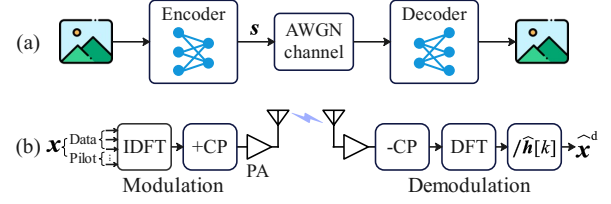


Fig. 2: (a) DeepJSCC workflow and (b) OFDM transmission process.

calibration [44]), the generated OFDM symbol after IDFT is

$$\mathbf{y} = \mathbf{F}^H \mathbf{x}^d + \mathbf{y}^p, \quad (1)$$

where $\mathbf{F} \in \mathbb{C}^{K^d \times K}$ denotes the truncated DFT matrix associated with the data symbols and \mathbf{y}^p corresponds to the data pilot. To combat inter-symbol interference, the last L entries of \mathbf{y} are appended to its beginning, forming the CP-extended signal, which is then transmitted through a power amplifier (PA). After propagating through the wireless channel, the received signal undergoes OFDM demodulation, which reverses the modulation process. The received data symbol is denoted as $\hat{\mathbf{z}}^d \in \mathbb{C}^{K^d}$, and $\hat{\mathbf{z}}^d[k] = \mathbf{h}[k]\mathbf{x}^d[k] + \mathbf{n}[k]$, where $\mathbf{h}[k]$ is channel gain at the k -th subcarrier and $\mathbf{n}[k]$ is additive Gaussian noise. To recover \mathbf{x}^d , the receiver utilizes the estimated channel $\hat{\mathbf{h}}[k]$ from preamble pilots to mitigate channel effects:

$$\hat{\mathbf{x}}^d[k] = (\mathbf{h}[k]\mathbf{x}^d[k] + \mathbf{n}[k]) / \hat{\mathbf{h}}[k]. \quad (2)$$

B. Direct Integration

The most straightforward approach to integrating DeepJSCC with OFDM is to directly use the continuous-valued features of the JSCC encoder as the input to the OFDM system. In this scheme, features are sequentially transmitted across different feature channels, with elements alternately mapped to the real and imaginary parts of the transmission symbols to maximize spectral efficiency. Fig. 3(a) presents the PSNR of this approach on an SDR platform for image transmission. While this scheme achieves a slight performance improvement over the conventional methods, its real-world performance on SDR falls significantly short of the ideal case (AWGN channel). This discrepancy highlights that the system fails to fully harness the potential of DeepJSCC in practical deployment. The primary limitations can be attributed to two fundamental factors.

First, in OFDM, symbols across different subcarriers are assumed to be statistically independent to ensure that deep fades (see Fig. 3(b)) do not simultaneously erase redundant information across multiple subcarriers. Otherwise, decoding accuracy would be severely degraded. However, as shown in Fig. 3(c), the elements in the feature \mathbf{s} generated by the JSCC encoder exhibit high correlation, with a correlation around 0.15 even at a separation of 40 elements. This correlation arises from the convolutional structure in the JSCC encoder, where adjacent elements

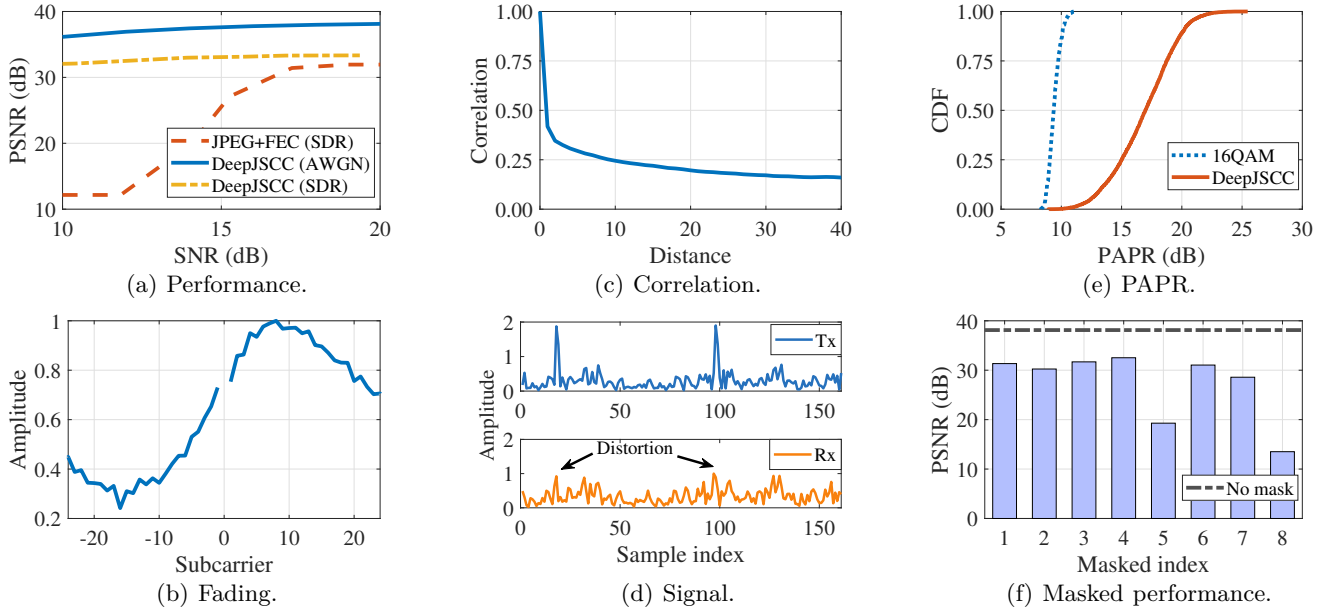


Fig. 3: (a) Performance over AWGN channel and an SDR platform, (b) frequency-selective fading, (c) correlation between two feature elements with different distances, (d) transmit and receive signals, (e) cumulative distribution function (CDF) of PAPR, and (f) performance after masking one channel.

in the sequence originate from neighboring regions of the original image. Such strong correlation contradicts the independence assumption of OFDM, increasing the risk of losing entire region information when deep fading occurs and thereby complicating reliable reconstruction at the receiver.

Second, the inherent correlation within the feature also contributes to an elevated PAPR. Given the limited dynamic range of the transmitter’s PA, high peaks in \mathbf{y} undergoes nonlinear distortion, as shown in Fig. 3(d), making it difficult for the receiver to accurately recover the symbols. Furthermore, the unconstrained nature of feature values generated by the JSCC encoder exacerbates this issue. As shown in Fig. 3(e), compared to OFDM with independently and randomly modulated 16QAM symbols, the direct integration of DeepJSCC and OFDM significantly increases the PAPR, leading to a deterioration in the performance.

Since both issues stem from the conflict between the feature’s inherent properties of the JSCC encoder and the fundamental assumption of OFDM, we propose two intermediary structures to mitigate these challenges: a feature-to-symbol mapping method (Section IV-A) and a cross-subcarrier precoding method (Section IV-B). These structures serve as a bridge for aligning the characteristics of JSCC encoding with the requirement of OFDM, thereby improving overall system performance.

C. Feasibility Study towards Flexibility

Users typically adjust their transmission requirements based on available bandwidth to prevent excessive delays. For example, adapting the video bitrate ensures smooth real-time playback. However, most existing JSCC encoders generally produce fixed-length outputs [12], [17], limiting

their flexibility to accommodate varying transmission conditions. To support variable bitrate control, existing approaches require training and storing an individual encoder-decoder pair for each bitrate level, which incurs significant overhead. Notably, the channel dimension of the output features encodes different aspects of the source content [45]. This means that even when only a subset of channels is transmitted, the original data can still be reconstructed, albeit with reduced fidelity. To verify this, we sequentially mask individual channels and assess the resulted reconstruction performance, as illustrated in Fig. 3(f). The results reveal that masking different channels leads to varying reconstruction quality, indicating that certain channels carry more critical information than others. When the available bandwidth is reduced, we can only transmit the critical channels for meeting latency requirements. However, how to pick out the critical channels and further improve the performance using them remains a challenge. To address this, Section IV-C introduces a novel progressive coding training strategy that prioritizes encoding essential information in earlier channels. It enables adaptive transmission, where the transmitter can dynamically decide whether to send the later channels based on real-time constraints, thereby meeting user requirements.

IV. The design of DeepStream

Our DeepStream is specifically designed to achieve efficient and noise-resilient real-time multimedia over OFDM. As illustrated in Fig. 4, DeepStream consists of two major components:

- Feature-to-symbol mapping (Section IV-A): It incorporates a flexible progressive coding strategy adapted

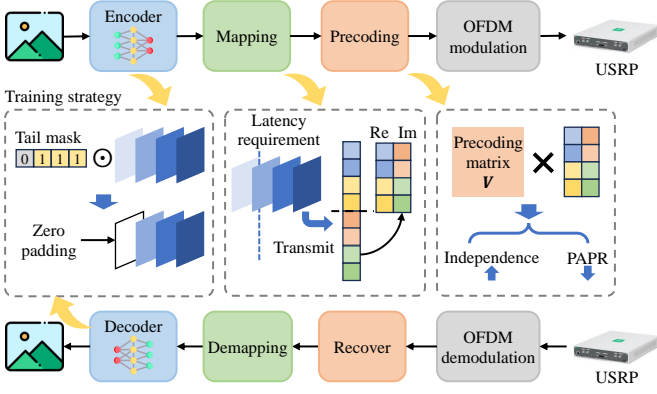


Fig. 4: Overview of DeepStream.

to varying latency requirements, and a mapping method from feature to symbol.

- Cross-subcarrier precoding method (Section IV-B): It performs symbol decorrelation and PAPR reduction via a tailored precoding matrix.

At the receiver, after OFDM demodulation, the signal undergoes inverse precoding and feature-to-symbol inversion before being processed by the JSCC decoder to accomplish the target task (e.g., image and video reconstruction). Furthermore, to support high-performance real-time multimedia transmission, we also develop the following fundamental components:

- Joint training strategy (Section IV-C). It ensures that critical information is concentrated in the earlier channels. Additionally, it optimizes both PAPR reduction and compression-reconstruction performance via a loss function.
- Real-time streaming framework (Section IV-D). It implements a dual-process streaming framework to support low-latency video streaming.

A. Feature-to-Symbol Mapping

In a wireless communication system, users have varying bandwidths, yet they all expect real-time multimedia transmission. To meet this requirement, the amount of transmitted data must be adjusted dynamically. Specifically, as shown in Fig. 5(a), given the number of subcarriers K , the length of CP L , and the user's allocated bandwidth B , the duration of one OFDM symbol is $(K+L)/B$. Among the K subcarriers, K^d subcarriers are allocated for data transmission. Consequently, the achievable symbol rate is $K^d B / (K+L)$. Unlike conventional coding and modulation schemes, DeepJSCC uses the JSCC encoder's output directly as the real and imaginary parts of the data symbols. When the required transmission latency is T^{\max} , the maximum transmittable feature length is

$$N = 2K^d B (T^{\max} - T^p) / (K+L), \quad (3)$$

where T^p is the latency occupied by the preamble pilots, and the factor of 2 accounts for both real and imaginary components carrying separate feature elements. According to the channel masking analysis in Section III-C, we can drop certain feature channels to meet the real-time

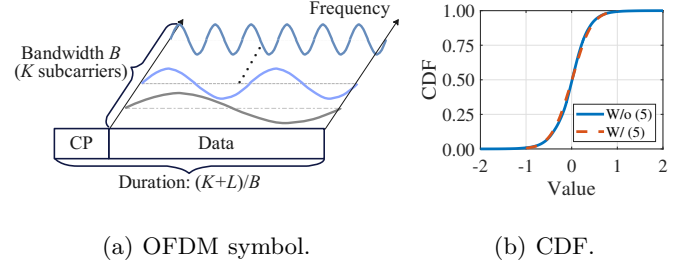


Fig. 5: (a) OFDM symbol structure and (b) value distribution of the encoder output features with/without the proposed activation function.

requirement T^{\max} , and the number of retained feature channels is

$$C^T = \left\lfloor \frac{2K^d B (T^{\max} - T^p)}{(K+L)HW} \right\rfloor, \quad (4)$$

where $\lfloor \cdot \rfloor$ represents the floor operation. Thanks to the training strategy proposed in Section IV-C, feature channels are ranked by importance, from highest to lowest. This implies that earlier channels carry more critical information. Therefore, given a selected number of channels C^T , only the first C^T channels are retained for transmission.

Due to the high PAPR issue, \mathbf{s} remains unsuitable for direct transmission, as the encoder's output is typically unconstrained. As shown in Fig. 5(b), the encoder output approximately follows a Gaussian distribution, leading to the occasional occurrence of extreme values. Such outliers induce nonlinear distortion in power amplifiers, thereby degrading overall system performance. This issue primarily stems from the absence of a suitable activation function. Among commonly used activation functions, ReLU does not impose an upper bound of the output, while Sigmoid and Tanh enforce range constraints but suffer from vanishing gradients at their boundaries [46]. As a result, none of these functions are well-suited for OFDM-based DeepJSCC. To address this issue, we propose an activation function that restricts the output range to $[-1, 1]$, as

$$f(x) = \min(\max(x, -1), 1). \quad (5)$$

By applying it, the encoder output is effectively limited to a predefined range. As illustrated in Fig. 5(b), under the same variance, the value range of the encoder's output features is significantly reduced, preventing extreme values and thereby mitigating PAPR. Furthermore, this activation function avoids the vanishing gradient issue, facilitating stable joint training of the encoder and decoder.

We now transform the feature into the data symbol \mathbf{x}^d . First, we segment the feature into multiple subsequences \mathbf{s} , each of length $2K^d$, and then map them into complex-valued sequences of length K^d . However, directly mapping elements in the features alternately to the real and imaginary parts of the data symbol would lead to a low spectral efficiency due to the high correlation between adjacent elements (see Fig. 3(c)). As shown in Fig. 6(a),

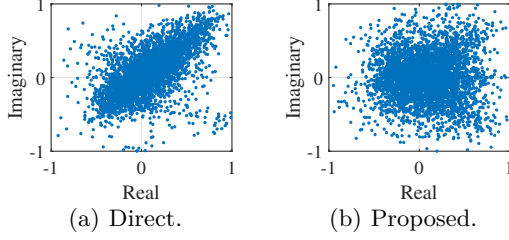


Fig. 6: The distribution of \mathbf{x}^d using (a) directly mapping and (b) the proposed method.

the resulting \mathbf{x} tends to cluster along the line $\text{Re}=\text{Im}$ in the complex plane. Consequently, the mapped symbols fail to fully exploit the available signal space, resulting in poor spectral efficiency. To address this problem, we propose a modified mapping strategy. Specifically, the first half of \mathbf{s} is assigned to the real component, while the second half is assigned to the imaginary component, with an alternating sign pattern, yielding \mathbf{x}^d :

$$\mathbf{x}^d[k] = \begin{cases} \mathbf{s}[k] + j\mathbf{s}[k + K^d], & k \text{ is odd,} \\ \mathbf{s}[k] - j\mathbf{s}[k + K^d], & k \text{ is even.} \end{cases} \quad (6)$$

As shown in Fig. 6(b), the resulting \mathbf{x}^d exhibits a more uniform distribution across the complex plane, effectively improving spectral efficiency.

B. Cross-subcarrier Precoding

To address the impact of correlation and reduce PAPR, we introduce a cross-subcarrier precoding matrix, denoted as $\mathbf{V} \in \mathbb{C}^{K^d \times K^d}$, where the precoded symbol is given by $\mathbf{x}^t = \mathbf{V}\mathbf{x}^d$. By appropriately designing \mathbf{V} , we aim to reduce symbol correlation across subcarriers, conforming to OFDM's fundamental assumption, while also shaping the transmit signal to prevent high PAPR. To this end, we first analyze the symbol correlation across subcarriers and the PAPR of the OFDM symbol, followed by an optimization-based design of \mathbf{V} .

Ensuring symbol independence across subcarriers helps counteract deep fading (see Fig. 3(b)). Ideally, transmitted symbols should be independent across all subcarriers to prevent correlated deep fades from erasing similar information. However, this requirement is overly stringent. In reality, fading correlation decreases with increasing frequency separation, meaning that strict independence is unnecessary for widely spaced subcarriers, as they do not experience similar fading conditions. To this end, we take subcarrier fading correlation into account and aim to minimize symbol correlation at the receiver.

Specifically, the received symbol at the k -th subcarrier is $\mathbf{h}[k]\mathbf{x}^t[k]$ when the noise is ignored, and the correlation between $\mathbf{h}[k_1]\mathbf{x}^t[k_1]$ and $\mathbf{h}[k_2]\mathbf{x}^t[k_2]$ can be expressed as

$$\begin{aligned} \rho[k_1, k_2] &= \frac{\mathbb{E}\{(\mathbf{h}[k_1]\mathbf{x}^t[k_1])(\mathbf{h}[k_2]\mathbf{x}^t[k_2])\}}{\text{Var}(\mathbf{h}[k]\mathbf{x}^t[k])} \\ &\stackrel{(*)}{=} \frac{\mathbb{E}\{\mathbf{h}[k_1]\mathbf{h}[k_2]\}\mathbb{E}\{\mathbf{x}^t[k_1]\mathbf{x}^t[k_2]\}}{\text{Var}(\mathbf{h}[k])\text{Var}(\mathbf{x}^t[k])} \\ &= \rho^h[k_1, k_2]\rho^{x,t}[k_1, k_2], \end{aligned} \quad (7)$$

where $(*)$ holds due to the independence between $\mathbf{x}^t[k]$ and $\mathbf{h}[k]$, ρ^h and $\rho^{x,t}$ represent the covariance matrices for \mathbf{h} and \mathbf{x}^t , respectively, and $\mathbb{E}\{\cdot\}$ is the operation of expectation. In the above expression, $\rho^{x,t}$ can be further given as: $\rho^{x,t} = \mathbf{V}\rho^{x,d}\mathbf{V}^H$, with $\rho^{x,d}$ being the covariance matrix for \mathbf{x}^d . Note that $\rho^{x,d}$ can be estimated over the training set of the JSCC encoder and decoder. For ρ^h , it can be assumed that subcarriers within the coherence bandwidth are fully correlated, while those beyond the coherence bandwidth are considered uncorrelated [47].¹ Let K^c denote the number of subcarriers within a coherence bandwidth, and ρ^h is a banded matrix with a bandwidth of K^c , where all nonzero elements are equal to 1.

For the PAPR issue, according to Eqn. (1), the OFDM symbol \mathbf{y} is expressed as: $\mathbf{y} = \mathbf{F}^H\mathbf{V}\mathbf{x}^d + \mathbf{y}^p$. Since designing a distinct precoding matrix for each OFDM symbol is infeasible due to the overhead of transmitting additional recovery information, we instead minimize the expected power at each sampling point, formulated as:

$$\begin{aligned} p^y[k] &= \mathbb{E}\{(\mathbf{f}_k^H\mathbf{V}\mathbf{x}^d + \mathbf{y}^p[k])(\mathbf{f}_k^H\mathbf{V}\mathbf{x}^d + \mathbf{y}^p[k])^H\} \\ &= p^t \mathbf{f}_k^H \rho^{x,t} \mathbf{f}_k + p^p[k], \end{aligned} \quad (8)$$

where $p^p[k] = \mathbf{y}^p[k](\mathbf{y}^p[k])^H$ is the transmit power of pilots \mathbf{y}^p , p^t is the transmit power of each data symbol, and \mathbf{f}_k is the k -th column vector of \mathbf{F} .

Given the above analysis, we can formulate the following problem to optimize the precoding matrix:

$$\min_{\mathbf{V}} \sum_{k_1, k_2} \rho^h[k_1, k_2]\rho^{x,t}[k_1, k_2] + \omega \max_k p^y[k], \quad \text{s.t. } \mathbf{V}\mathbf{V}^H = \mathbf{I}, \quad (9)$$

where ω is a weighting factor balancing PAPR reduction and the unitary constraint on \mathbf{V} ensures that the transmit power per each subcarrier remains unchanged. This problem is non-convex due to the non-convex objective function

¹The coherence bandwidth depends on the environment, and typical values can be adopted following the existing 4G/5G standards [48].

Algorithm 1: Optimization for Precoding Matrix

Input: Covariance matrices ρ^h for channel and $\rho^{x,d}$ for data symbol, and the number of random initializations N^r .

Output: Precoding matrix \mathbf{V} .

```

1 for  $n = 1, \dots, N^r$  do
2   Randomly initialize  $\mathbf{V}$ ;
3   for  $k = 1, \dots, K^d$  do
4     obtain  $\mathbf{v}_k$  by solving the problem with
        $\mathbf{v}_k \mathbf{v}_{k'}^H = 0, k' < k$  and  $\|\mathbf{v}_k\|^2 \leq 1$ ;
5      $\mathbf{v}_k \leftarrow \mathbf{v}_k / \|\mathbf{v}_k\|$ ;
6   end
7   Construct  $\mathbf{V}_n$  and calculate the corresponding
     objective function value  $O_n$ .
8 end
9 Compare the  $N^r$  objective values and select the  $\mathbf{V}$ 
  corresponding to the minimum one as the output.
```

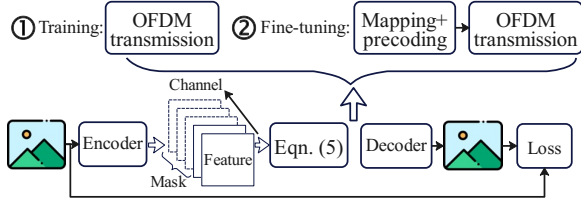


Fig. 7: Two-step training strategy.

and constraint. To address this problem, we leverage the alternating optimization method [49]. Considering the structure of $\rho^h[k_1, k_2]$, we optimize each row vector of \mathbf{V} sequentially. Specifically, when optimizing the k -th row vector, i.e., \mathbf{v}_k , the objective function is convex because $\sum_{k_1, k_2} \rho^h[k_1, k_2]$ is a quadratic function of \mathbf{v}_k with a positive quadratic term and $\mathbf{p}^u[k]$ follows the same convex property. The unitary constraint is decomposed into two separate constraints: one requires \mathbf{v}_k to be orthogonal to the previous $(k-1)$ column vectors, i.e., $\mathbf{v}_k \mathbf{v}_{k'}^H = 0$, $k' < k$, which is convex, while the other enforces the norm of \mathbf{v}_k to be 1, i.e., $\|\mathbf{v}_k\|^2 = 1$, which is non-convex. To handle the non-convex constraint, we first relax the non-convex constraint into a convex one: $\|\mathbf{v}_k\|^2 \leq 1$, and then optimize \mathbf{v}_k using existing convex solvers, such as CVX [50]. The resulting \mathbf{v}_k is then normalized to satisfy the original constraint. After K steps, the final precoding matrix \mathbf{V} is obtained. Additionally, to further minimize the objective function, we initialize multiple instances of \mathbf{V} randomly and apply the optimization process to each. The solution with the lowest objective function value is selected as the final \mathbf{V} . The complete optimization procedure is outlined in Algorithm 1. Notably, the proposed optimization process is primarily related to the type of transmission task (associated with $\rho^{x,d}$) and the wireless environment (associated with ρ^h). Therefore, Algorithm 1 is executed once before deploying DeepStream, after which no further updates are required.

C. Joint Training Strategy

To ensure the effectiveness of DeepJSCC and the designs in Sections IV-A and IV-B over real-world channels, we propose a two-step training strategy, as shown in Fig. 7. The first step is the progressive coding and decoding training over the multipath channel, aiming to concentrate critical information in the earlier channels. This step ensures the system's ability to handle varying latency and QoS requirements. The second step is fine-tuning to adapt to the proposed mapping and precoding methods.

In the first step, to ensure that critical information is concentrated in the earlier channels, we randomly generate a mask length C^m ($C^m < C$) in each training iteration. The last C^m feature channels in the encoder output are then discarded and replaced with zeros to maintain dimensional consistency. The modified feature is subsequently fed into the JSCC decoder for reconstruction. For image/video reconstruction tasks, we use mean squared

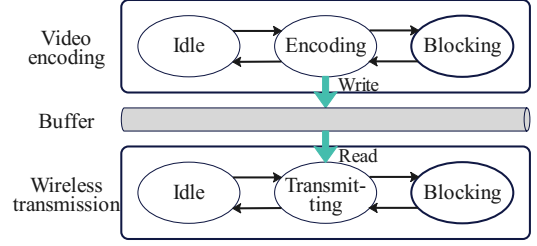


Fig. 8: Dual-process streaming framework at the transmitter.

error (MSE) as the loss function, ensuring that the decoder learns to restore the original input with high fidelity. Through this training approach, the encoder naturally prioritizes encoding important information into earlier channels, while the decoder learns to adapt to such feature distributions, improving overall performance.

Before starting the second step, we first use the trained encoder and decoder from the first step to estimate the covariance matrix of \mathbf{x}^d , which is subsequently used to calculate the precoding matrix \mathbf{V} . Next, we proceed with the second step, where the JSCC encoder and decoder are fine-tuned to adapt to OFDM transmission. The channel state information (CSI) samples for fine-tuning are randomly sampled. This fine-tuning process incorporates the mapping method and activation function from Section IV-A, as well as the OFDM transmission process with the precoding matrix from Section IV-B. Additionally, to mitigate the PAPR issue, we introduce a weighted loss function combining MSE and PAPR [32], formulated as:

$$\mathcal{L} = \alpha \text{MSE} + (1 - \alpha) \text{PAPR}. \quad (10)$$

This ensures a balance between reconstruction accuracy and PAPR reduction, enhancing both semantic fidelity and transmission efficiency.

D. Real-Time Streaming

Before deploying the JSCC encoder and decoder after training, we can further reduce hardware overhead through quantization. Since our feature transmission method resembles analog transmission, the feature SNR is inherently limited by the resolution of the SDR's ADC and DAC. Given that the precision of ADC and DAC is typically limited to 16 bits, we apply 16-bit floating-point quantization to the model (originally 32-bit). This significantly reduces encoding and decoding latency while maintaining near-identical performance.

For image transmission, we adopt a sequential transmission approach, where the JSCC encoder first extracts features, followed by wireless transmission using SDR. At the receiver, the signal is demodulated and decoded to complete the reconstruction task. Unlike image transmission, video transmission requires continuous frame transmission to enable real-time streaming. A sequential approach would introduce high latency, as each frame would need to wait for the previous frame to be fully decoded. To address this issue, we employ a dual-process

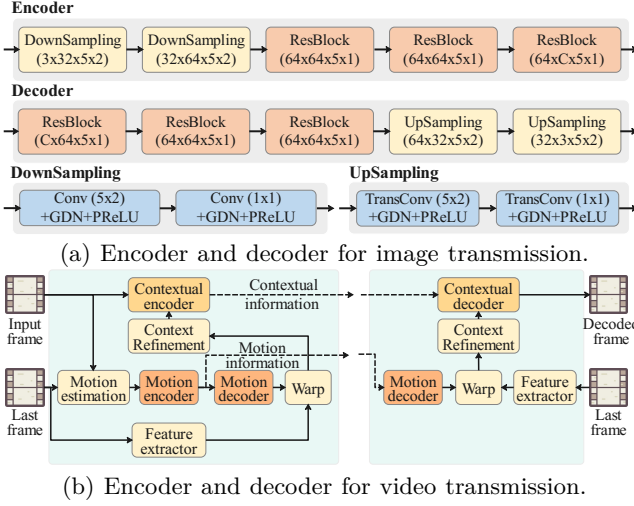


Fig. 9: Encoder and decoder for (a) image transmission and (b) video streaming.

parallel streaming framework, as illustrated in Fig. 8. In this framework, one process handles video encoding, while the other manages wireless transmission, with a buffer serving as temporary storage for the encoded features. Specifically, the first process (video encoding) operates in three states: idle, encoding, and blocking. In the idle state, it waits for a new frame to arrive. Once a frame arrives, it enters the encoding state, where the JSCC encoder compresses the frame into features and writes them to the buffer. If the buffer is full, the process enters the blocking state, waiting until the buffer becomes available before returning to the encoding state. After writing data, it transitions back to the idle state, ready to process the next incoming frame. In the second process for wireless transmission, there are also three states: idle, transmitting, and blocking. Different from the first process, the transmitting state involves mapping, precoding, OFDM modulation, and signal transmission. The blocking state occurs when the process waits for the channel to become available before continuing to transmit. At the receiver, a similar framework is employed for reconstruction, with implementation details omitted for brevity.

V. Implementation and Setup

In this section, we first elaborate on DeepStream's implementation and then introduce the experiment setup.

A. System Implementation

In this paper, we consider image transmission and video streaming as two representative multimedia applications. The architecture and training details of the JSCC encoder and decoder are described below.

Image transmission. As shown in Fig. 9(a), The JSCC encoder consists of five convolutional layers, including three residual layers [51] and two downsampling layers, which reduce the feature's width and height to 1/4 of the original image. The number of channels is set to 12. Similarly, the decoder is also built with five convolutional

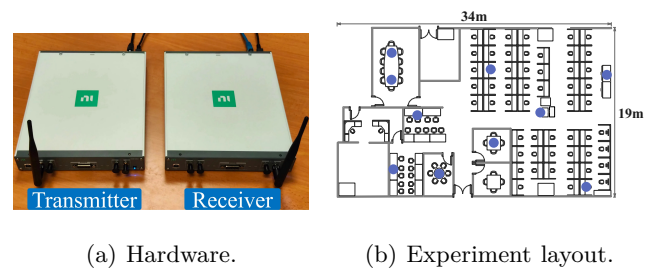


Fig. 10: DeepStream implementation: (a) hardware configurations and (b) experiment layout.

layers, and the downsampling layers are replaced with upsampling layers to ensure that the reconstructed image retains the original dimensions. Both JSCC encoder and decoder are implemented in Python 3.8 with PyTorch 1.13 and trained on a Linux server equipped with RTX A6000 GPUs, following the training strategy in Section IV-C. The UCF-101 dataset [52] is used for training and testing, where images are randomly cropped to 256×256 pixels. Adam optimizer is adopted, with a learning rate of 5×10^{-4} and a batch size of 32.

Video streaming. For video streaming, we handle the transmission of both keyframes (I-frames) and predicted frames (P-frames). Following [23], we set the group-of-pictures (GOP) size as 4. Since I-frames require direct frame transmission, we adopt the image transmission approach with C being 8. For P-frames, instead of transmitting the entire frame, we transmit only the differences relative to the previous frame, thereby reducing the transmission load. To achieve this, we adopt the method proposed in [53]. As shown in Fig. 9(b), this method extracts and transmits motion features and contextual features sequentially. Both motion and contextual information are downsampled to 1/16 of the original image's height and width, with the number of motion feature channels and contextual feature channels set to 16 and 64, respectively. The training process follows the same procedure as image transmission, using the UCF-101 dataset with a learning rate of 1×10^{-4} and a batch size of 8.

With the trained encoder and decoder, we implement a DeepStream prototype using two USRP X310 devices [54] and two workstations, as shown in Fig. 10(a). One pair of USRP and a workstation serve as the transmitter, while the other functions as the receiver. We utilize the USRP Hardware Driver (UHD) [55] to manage signal transmission and reception. Both USRP devices operate at a center frequency of 2.4 GHz with a bandwidth of 10 MHz. Following the general OFDM configurations [56], the system employs 64 subcarriers, with 48 allocated for data symbols, 4 for data pilot, and 12 left unused. The default transmission latency constraint is set to 3 ms.

B. Experiment Setup

We conduct experiments in an office environment, as illustrated in Fig. 10(b). Ten locations are selected as transmitter and receiver positions to measure the average performance under different SNR conditions in both line-

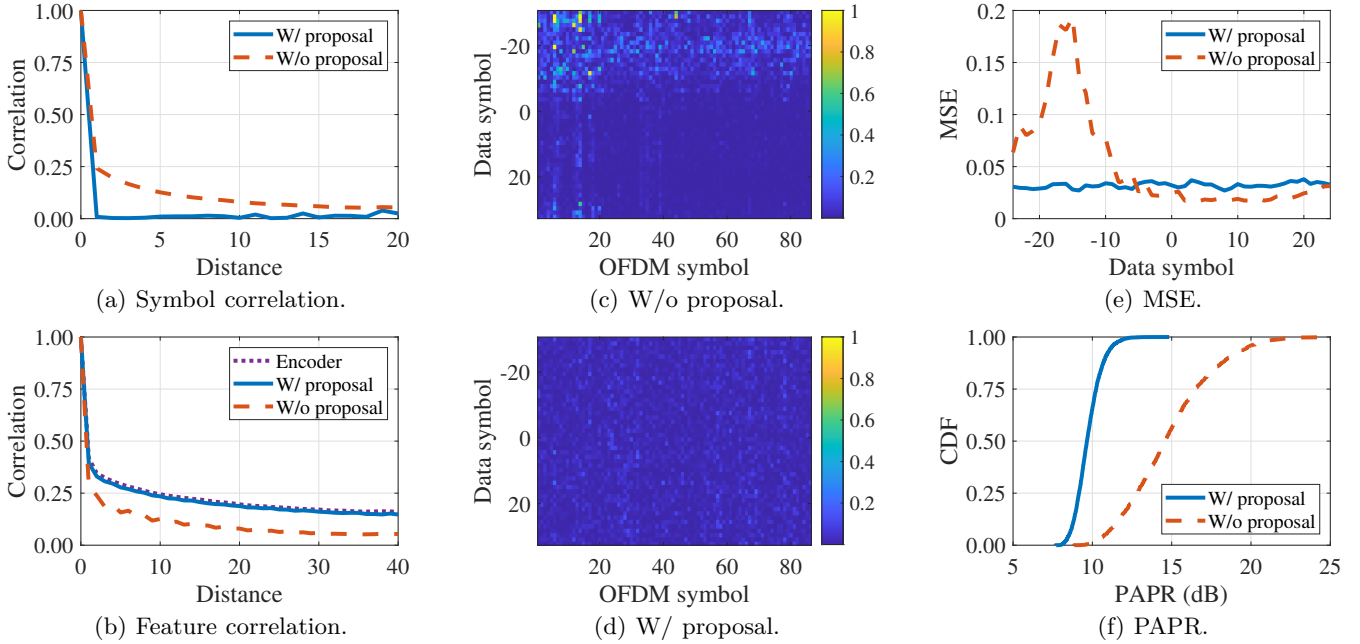


Fig. 11: Performance of the proposed mapping and precoding methods: (a) symbol correlation, (b) correlation between two feature elements, (c) and (d) squared error across different subcarriers and OFDM symbols, (e) MSE across data symbols, and (f) PAPR.

of-sight (LoS) and non-line-of-sight (NLoS) scenarios. The total over-the-air measurement duration exceeds 11 hours.

For image transmission, we consider two baselines: i) direct deployment of existing DeepJSCC [12], where the same neural network mentioned in Section V-A is adopted without our proposed modifications and further trained with OFDM; ii) standard image codecs, where JPEG is used for source coding, low-density parity-check (LDPC) code [57] is adopted for channel coding with a block length of 672 and a code rate of 1/2 [18], and 16QAM is applied for OFDM transmission. Following [12], when JPEG decoding fails, the image is reconstructed using the mean pixel value for each channel.

For video transmission, we also consider two baselines: i) direct deployment of existing DeepJSCC [53], where the same neural network mentioned in Section V-A is adopted without our proposal and further trained with OFDM; ii) standard video codecs, where H.264 is adopted for source coding, LDPC code is employed for channel coding, and 16-QAM is used for modulation.

To ensure a fair comparison, all schemes are evaluated under the same transmission latency during the experiment. The compression ratios of JPEG and H.264 are adjusted according to the channel code rate and modulation order to meet the transmission latency requirement. For image transmission, PSNR is employed as the performance metric. For video transmission, we adopt the multiscale structural similarity index measure (MS-SSIM) to evaluate the quality of the reconstructed frames. Following recent work [22], we express MS-SSIM in dB using the formula $-10 \log(1 - \text{MS-SSIM})$.

VI. Evaluation

We start with three micro-benchmark studies to demonstrate the effectiveness of each component in DeepStream and then present the overall performance.

A. Micro-benchmark Studies

1) Mapping and precoding: To evaluate the effectiveness of the feature-to-symbol mapping and precoding methods proposed in Sections IV-A and IV-B, Fig. 11(a) presents the symbol correlation between two different subcarriers at the receiver. One can see that, the proposed mapping and precoding methods significantly reduce the correlation compared to the baseline without these techniques, meeting the requirements of OFDM. Additionally, Fig. 11(b) illustrates the correlation between elements in the demodulated feature at the receiver. The results show that, compared to the baseline, the feature correlation better aligns with that generated by the JSCC encoder, demonstrating that the characteristic of feature is well preserved after OFDM modulation and wireless transmission. This property enhances information recovery performance at the JSCC decoder.

To further assess the effectiveness of the mapping and precoding methods, we present the squared error of different data symbols across various OFDM symbols, as shown in Figures 11(c) and 11(d). Without the proposed methods, each data symbol at the same position within an OFDM symbol corresponds to a fixed subcarrier, making it susceptible to deep fading, as shown in Fig. 11(c). The figure reveals that data symbols on certain subcarriers experience high squared error, while some OFDM symbols exhibit consistently high squared error due to

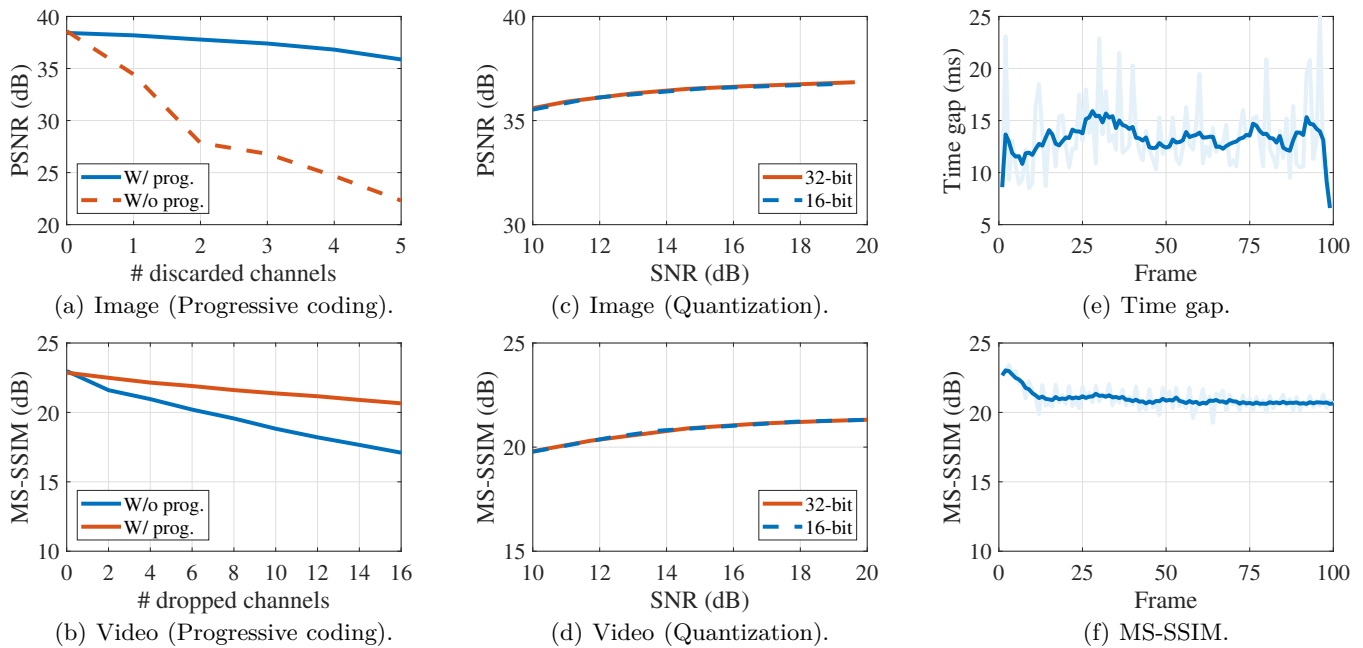


Fig. 12: Performance of (a) image and (b) video transmission with different number of discarded channels, and performance with/without quantization for (c) image transmission and (d) video streaming, and video streaming: (e) time gap between adjacent frames and (f) MS-SSIM of each frame.

nonlinear distortion caused by high PAPR. In contrast, as depicted in Fig. 11(d), the proposed methods effectively mitigate squared error fluctuations, leading to a more stable transmission. Furthermore, Fig. 11(e) shows the MSE across different data symbol positions over multiple OFDM symbols, confirming that our method equalizes the error distribution, thereby preventing localized information loss. Finally, Fig. 11(f) depicts the CDF of PAPR, demonstrating a substantial reduction in PAPR when applying our method. These results collectively validate the effectiveness of the proposed mapping and precoding methods in mitigating subcarrier correlation, reducing squared error, and improving transmission robustness.

2) Progressive coding: We now validate the effectiveness of the progressive encoding strategy. We discard a portion of the later channels in the feature, and then directly feed the remaining features into the decoder for reconstruction after undergoing the channel. Fig. 12(a) illustrates the image transmission performance under different numbers of discarded channels. For comparison, we also present the performance of a baseline scheme without progressive coding. As shown in the figure, although both schemes experience performance degradation as more channels are discarded, our proposed strategy exhibits a significantly slower decline. Even when five channels are discarded, the performance loss of our scheme remains within 3 dB, whereas the baseline suffers a 16 dB drop. We further evaluate the effectiveness of progressive encoding in video transmission, focusing on P-frames, as shown in Fig. 12(b). Here, the number of discarded channels refers to the total number of motion and contextual channels, each contributing equally. The results confirm that our proposal also outperforms the baseline. When 16 channels

are discarded, our scheme incurs only a 2.2 dB performance loss, whereas the baseline suffers a 5.8 dB loss. These results underscore the effectiveness of the progressive encoding strategy in maintaining high QoS. In the sequel, the number of motion feature channels and contextual feature channels is set to 8 and 56, respectively.

3) Quantization and video streaming: Before conducting the streaming tests, we first present the results when the encoder and decoder are quantized to 16-bit floating-point precision in Fig. 12(c) and Fig. 12(d). The figure demonstrates that for both image and video transmission, the quantized encoder and decoder achieve nearly identical performance to the original 32-bit floating-point ones across different SNRs. This can be attributed to the inherent quantization limitations of the USRP’s ADC and DAC, which dictate the overall system precision. Therefore, as long as the model’s quantization bit width is not lower than the precision of the ADC and DAC, performance remains virtually unaffected.

We next evaluate the real-time video streaming performance of DeepStream. Fig. 12(e) depicts the time gap between the completion of consecutive frame decodings at the receiver, where most gaps fall within 20 ms. For a 30 FPS video (frame interval of 33 ms), this gap satisfies the real-time playback requirement, validating the effectiveness of our dual-process framework. Furthermore, Fig. 12(f) presents the MS-SSIM of each decoded frame. The results show consistently high MS-SSIM values, providing initial evidence of DeepStream’s superior performance. In the next section, we will further evaluate DeepStream’s performance.

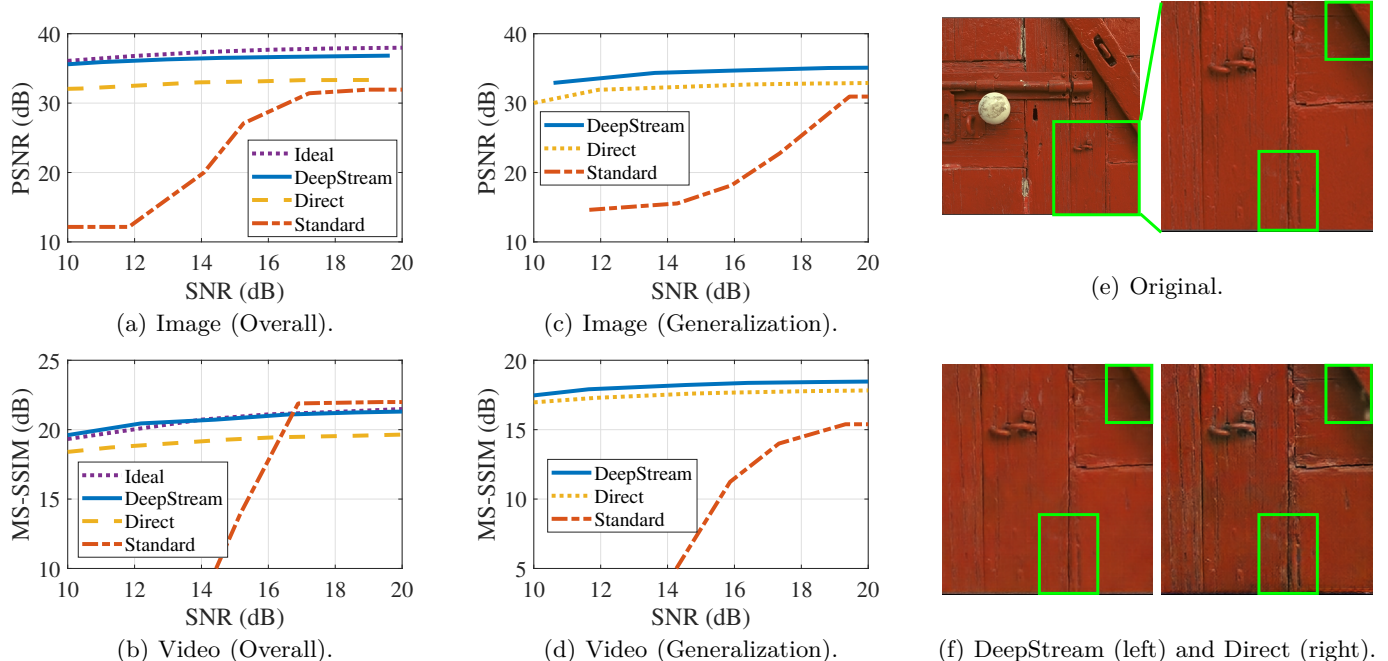


Fig. 13: Performance under various SNRs for (a) image transmission and (b) video streaming, and generalization performance for (c) image transmission with Kodak dataset and (d) video streaming with HEVC Class D dataset, (e) and (f) an image example under DeepStream and direct deployment scheme.

B. End-to-end Performance

1) Overall performance: Fig. 13(a) and Fig. 13(b) present the performance of image transmission and video streaming under different SNR conditions in the LoS scenario. For image transmission, all schemes experience performance degradation as the SNR decreases. However, the decline is significantly slower for all DeepJSCC-based schemes compared to the standard scheme. Notably, at a lower SNR level, the standard scheme suffer from the cliff effect, whereas DeepJSCC approaches maintain relatively high performance. Moreover, DeepStream demonstrates a significant performance improvement over the direct deployment of DeepJSCC. At an SNR of 10 dB, DeepStream achieves an approximate 3 dB performance gain. To assess whether DeepStream fully exploits the potential of DeepJSCC, we compare its performance against the ideal case under AWGN conditions. The results indicate that DeepStream closely approaches the ideal performance, with a maximum loss of only 1 dB. Similarly, Fig. 13(b) presents the results for video transmission, revealing a comparable trend. Specifically, the standard scheme outperforms the DeepJSCC-based schemes at high SNR regimes. However, its performance deteriorates rapidly as the SNR decreases, whereas the DeepJSCC schemes maintain robust performance in low-SNR regimes. Moreover, DeepStream consistently outperforms the direct deployment scheme, thereby validating the effectiveness of the proposed framework.

2) Generalization performance: To verify the generalizability of DeepStream, we conduct experiments from both dataset and channel perspectives. For image transmission,

we train the model on the ImageNet dataset [58] and evaluate on the Kodak dataset [59]. For video streaming, we train the model on the Vimeo-90K dataset [60] and evaluate on the HEVC Class D dataset [61]. Fig. 13(c) and Fig. 13(d) present the performance of image transmission and video streaming. Across different SNR levels, DeepStream consistently outperforms other schemes on the new datasets. This indicates that even when using the pre-trained model and the precomputed precoding matrix, the proposed scheme still performs well on unseen data, validating its generalizability.

To further investigate performance, Fig. 13(e) and Fig. 13(f) present image transmission results of both the direct deployment scheme and DeepStream for the same image at an SNR of about 10dB. In the direct deployment scheme, noticeable distortions appear in the lower regions, where details deviate significantly from the original image. Additionally, significant blurring occurs in the upper right corner. In contrast, the image reconstructed by DeepStream closely resembles the original, achieving a higher PSNR, thereby demonstrating its effectiveness.

We further evaluate the performance of DeepStream in the NLoS scenario. To assess whether the trained encoder and decoder generalize beyond specific channel conditions, we conduct image transmission and video streaming experiments in the NLoS scenario. Fig. 14(a) and Fig. 14(b) present the results. In the NLoS scenario, all schemes demonstrate performance degradation compared with the results in the LoS scenario, but DeepStream still outperforms both baselines and achieves performance comparable to its results in the LoS scenario, as shown

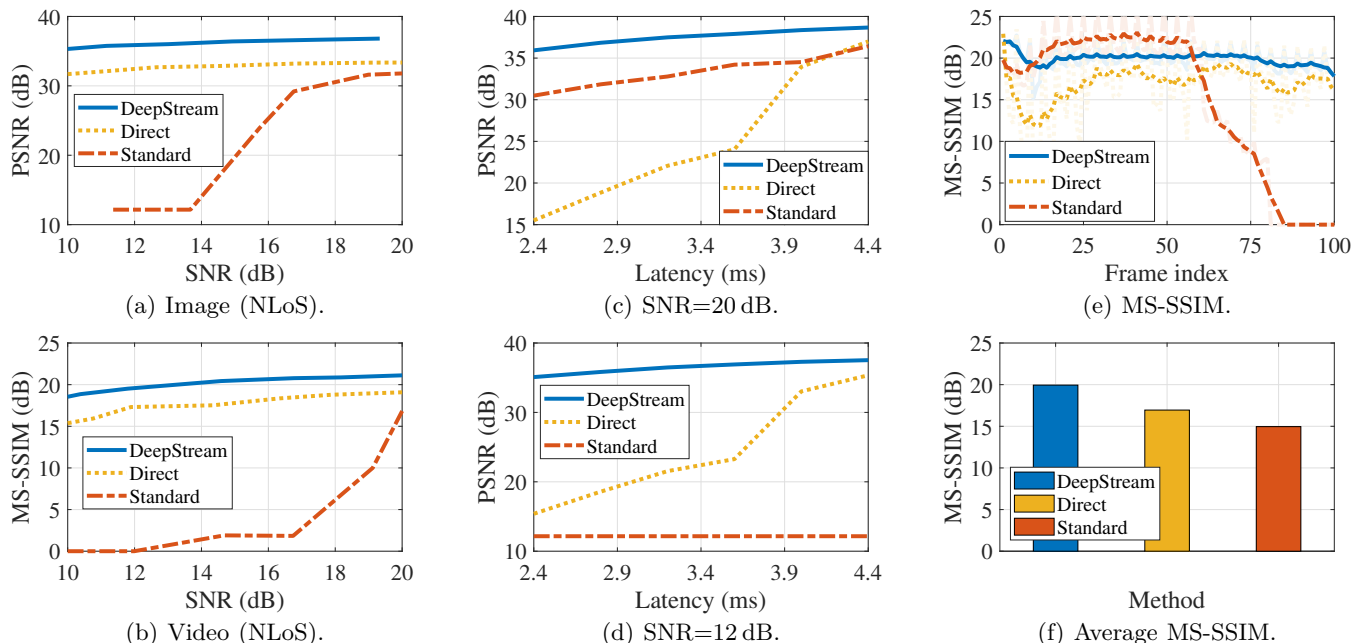


Fig. 14: Performance for (a) image transmission and (b) video streaming in the NLoS scenario, and performance for image transmission under different latency constraints at high (c) and low (d) SNRs, and performance for video streaming with mobility: (e) MS-SSIM of each frame and (f) average MS-SSIM.

in Fig. 13(a) and Fig. 13(b). These results demonstrate that the proposed scheme maintains robust performance across diverse channel conditions, further validating its generalizability.

3) Performance with varying latency: Fig. 14(c) and Fig. 14(d) present the image transmission performance under varying latency constraints. At high SNRs in Fig. 14(c), all three schemes experience performance degradation as the latency constraint tightens due to reduced data transmission capacity. Notably, DeepStream shows a significantly slower decline compared to the direct deployment scheme. This is because the progressive encoding strategy effectively prioritizes important information, making it better suitable for urgent transmission requirements. Furthermore, DeepStream consistently outperforms the standard scheme, demonstrating the advantages of DeepJSCC in leveraging DL for efficient compression and reconstruction using critical information.

Meanwhile, at low SNRs in Fig. 14(d), performance degradation is more pronounced due to poor channel conditions. The standard scheme undergoes a substantial performance drop and, even under loose latency constraints, fails to decode correctly, resulting in only minimal PSNR. In contrast, DeepJSCC-based schemes (DeepStream and direct deployment) sustain relatively high performance, benefiting from their inherent robustness and superior error correction capabilities.

4) Performance with mobility: To further assess the effectiveness of DeepStream in dynamic environments, we evaluate its performance in a mobile scenario. Specifically, we fix the location of the transmitter and the movement trajectory of the receiver, transitioning from a location with an SNR of about 20 dB to one with about 12 dB.

The corresponding results for video streaming are shown in Fig. 14(e) and Fig. 14(f). As shown in the results, all three schemes undergo performance degradation as the receiver moves, primarily due to the decreasing SNR. The standard scheme is highly sensitive to channel fluctuations, resulting in significant performance degradation. In contrast, both DeepStream and the direct deployment scheme maintain more stable performance, demonstrating robustness against mobility and fluctuating channel conditions. Furthermore, DeepStream surpasses the direct deployment scheme, further validating its effectiveness in mobile scenarios.

VII. Discussion

While most existing works show promising results, their evaluations remain limited to simulations, leaving real-world feasibility uncertain. To bridge this gap, we introduce DeepStream, a prototype system for DeepJSCC. Our primary objective is to integrate DeepJSCC with OFDM systems and fully exploit its potential. We focus on intermediate-layer designs that effectively align the JSCC encoding process with OFDM transmission. Although we do not modify the encoder or decoder directly, our system remains compatible with a wide range of existing neural network architectures. For instance, recent advances such as vision transformers (ViT) [25] and diffusion models [62], have been employed to further improve the transmission efficiency of DeepJSCC systems in image transmission. Likewise, ViT-based architectures have also shown promise in video transmission [22]. By integrating the proposed feature-to-symbol mapping method and the cross-subcarrier precoding technique, these models can be made more compatible with OFDM-based transmission. We note that while these approaches yield significant performance

gains in simulation, they often incur considerable computational overhead, limiting their suitability for real-time applications. Therefore, we do not consider these networks in this work. Nonetheless, they can be incorporated into our framework for delay-tolerant applications. Enabling real-time transmission under such architectures remains a critical challenge, motivating future work on designing high-capacity yet efficient neural networks that strike a favorable balance between performance and complexity. Lastly, as a pioneering effort, our work primarily addresses latency and technical challenges at the physical layer. Nevertheless, our framework can be seamlessly extended to broader deployment scenarios by incorporating network-induced latency considerations [63] and additional technologies (e.g., multiple-input and multiple-output [25] and cooperative relay networks [64]).

VIII. Conclusion

In this paper, we have prototyped DeepStream, a real-time noise-resilient DeepJSCC system designed for efficient and robust multimedia transmission. To enhance the compatibility of DeepJSCC with OFDM systems, we introduce a feature-to-symbol mapping method and a cross-subcarrier precoding technique. Additionally, we develop a progressive coding strategy to improve transmission flexibility under varying latency constraints. Extensive evaluations have demonstrated that DeepStream consistently outperforms baseline methods across a wide range of SNRs, particularly in low-SNR conditions. By bridging the gap between theoretical advancements and practical implementation, DeepStream takes a significant step toward the real-world deployment of DeepJSCC systems.

References

- [1] X. D. Duan, X. Y. Wang, L. Lu, N. X. Shi, C. Liu, T. Zhang, and T. Sun, "6g architecture design: from overall, logical and networking perspective," *IEEE Commun. Mag.*, vol. 61, no. 7, pp. 158–164, 2023.
- [2] W. Chen, X. Lin, J. Lee, A. Toskala, S. Sun, C. F. Chiasserini, and L. Liu, "5g-advanced toward 6g: Past, present, and future," *IEEE J. Sel. Areas Commun.*, vol. 41, no. 6, pp. 1592–1619, 2023.
- [3] C.-X. Wang, X. You, X. Gao, X. Zhu, Z. Li, C. Zhang, H. Wang, Y. Huang, Y. Chen, H. Haas et al., "On the road to 6g: Visions, requirements, key technologies, and testbeds," *IEEE Commun. Surveys Tuts.*, vol. 25, no. 2, pp. 905–974, 2023.
- [4] 3GPP, "Unmanned Aerial System (UAS) support in 3GPP," <http://www.3gpp.org/DynaReport/22125.htm>, 2024, online; accessed: 16 January 2025.
- [5] J. Ballé, D. Minnen, S. Singh, S. J. Hwang, and N. Johnston, "Variational image compression with a scale hyperprior," in *Proc. Int. Conf. Learn. Represent. (ICLR)*, 2018, pp. 1–23.
- [6] J. Shao, Y. Mao, and J. Zhang, "Learning task-oriented communication for edge inference: An information bottleneck approach," *IEEE J. Sel. Areas Commun.*, vol. 40, no. 1, pp. 197–211, 2021.
- [7] K. Du, A. Pervaiz, X. Yuan, A. Chowdhery, Q. Zhang, H. Hoffmann, and J. Jiang, "Server-driven video streaming for deep learning inference," in *Proc. ACM SIGCOMM Conf.*, 2020, pp. 557–570.
- [8] Y. Li, A. Padmanabhan, P. Zhao, Y. Wang, G. H. Xu, and R. Netravali, "Reducto: On-camera filtering for resource-efficient real-time video analytics," in *Proc. ACM SIGCOMM Conf.*, 2020, pp. 359–376.
- [9] D. J. MacKay, "Fountain codes," *IEE Proceedings-Communications*, vol. 152, no. 6, pp. 1062–1068, 2005.
- [10] D. Gündüz, Z. Qin, I. E. Aguerri, H. S. Dhillon, Z. Yang, A. Yener, K. K. Wong, and C.-B. Chae, "Beyond transmitting bits: Context, semantics, and task-oriented communications," *IEEE J. Sel. Areas Commun.*, vol. 41, no. 1, pp. 5–41, 2022.
- [11] X. Luo, H.-H. Chen, and Q. Guo, "Semantic communications: Overview, open issues, and future research directions," *IEEE Wireless Comm.*, vol. 29, no. 1, pp. 210–219, 2022.
- [12] E. Bourtsoulatz, D. B. Kurka, and D. Gündüz, "Deep joint source-channel coding for wireless image transmission," *IEEE Trans. Cogn. Commun. Netw.*, vol. 5, no. 3, pp. 567–579, 2019.
- [13] D. Gündüz, M. A. Wigger, T.-Y. Tung, P. Zhang, and Y. Xiao, "Joint source-channel coding: Fundamentals and recent progress in practical designs," *Proc. IEEE*, 2024.
- [14] J. Dai, S. Wang, K. Tan, Z. Si, X. Qin, K. Niu, and P. Zhang, "Nonlinear transform source-channel coding for semantic communications," *IEEE J. Sel. Areas Commun.*, vol. 40, no. 8, pp. 2300–2316, 2022.
- [15] D. B. Kurka and D. Gündüz, "Deepjscc-f: Deep joint source-channel coding of images with feedback," *IEEE J. Sel. Areas Inf. Theory*, vol. 1, no. 1, pp. 178–193, 2020.
- [16] D. Huang, F. Gao, X. Tao, Q. Du, and J. Lu, "Toward semantic communications: Deep learning-based image semantic coding," *IEEE J. Sel. Areas Commun.*, vol. 41, no. 1, pp. 55–71, 2022.
- [17] J. Xu, B. Ai, W. Chen, A. Yang, P. Sun, and M. Rodrigues, "Wireless image transmission using deep source channel coding with attention modules," *IEEE Trans. Circuits Syst. Video Technol.*, vol. 32, no. 4, pp. 2315–2328, 2021.
- [18] S. Tang, Q. Yang, L. Fan, X. Lei, A. Nallanathan, and G. K. Karagiannis, "Contrastive learning based semantic communications," *IEEE Trans. Commun.*, vol. 72, no. 10, pp. 6328–6343, 2024.
- [19] E. Erdemir, T.-Y. Tung, P. L. Dragotti, and D. Gündüz, "Generative joint source-channel coding for semantic image transmission," *IEEE J. Sel. Areas Commun.*, vol. 41, no. 8, pp. 2645–2657, 2023.
- [20] T. Han, Q. Yang, Z. Shi, S. He, and Z. Zhang, "Semantic-preserved communication system for highly efficient speech transmission," *IEEE J. Sel. Areas Commun.*, vol. 41, no. 1, pp. 245–259, 2022.
- [21] Z. Weng and Z. Qin, "Semantic communication systems for speech transmission," *IEEE J. Sel. Areas Commun.*, vol. 39, no. 8, pp. 2434–2444, 2021.
- [22] S. Wang, J. Dai, Z. Liang, K. Niu, Z. Si, C. Dong, X. Qin, and P. Zhang, "Wireless deep video semantic transmission," *IEEE J. Sel. Areas Commun.*, vol. 41, no. 1, pp. 214–229, 2022.
- [23] T.-Y. Tung and D. Gündüz, "Deepwive: Deep-learning-aided wireless video transmission," *IEEE J. Sel. Areas Commun.*, vol. 40, no. 9, pp. 2570–2583, 2022.
- [24] M. Yang, C. Bian, and H.-S. Kim, "Ofdm-guided deep joint source channel coding for wireless multipath fading channels," *IEEE Trans. Cogn. Commun. Netw.*, vol. 8, no. 2, pp. 584–599, 2022.
- [25] H. Wu, Y. Shao, C. Bian, K. Mikolajczyk, and D. Gündüz, "Deep joint source-channel coding for adaptive image transmission over mimo channels," *IEEE Trans. Wireless Commun.*, vol. 23, no. 10, pp. 15 002–15 017, 2024.
- [26] X. Mu, Y. Liu, L. Guo, and N. Al-Dhahir, "Heterogeneous semantic and bit communications: A semi-noma scheme," *IEEE J. Sel. Areas Commun.*, vol. 41, no. 1, pp. 155–169, 2022.
- [27] K. Chi, Q. Yang, Z. Yang, Y. Duan, and Z. Zhang, "Capacity optimizing resource allocation in joint source-channel coding systems with qos constraints," *IEEE Trans. Commun.*, vol. 73, no. 6, pp. 4198–4212, 2025.
- [28] Y. Liu, C. Ouyang, Z. Ding, and R. Schober, "The road to next-generation multiple access: A 50-year tutorial review," *Proc. IEEE*, 2024.
- [29] Y. G. Li and G. L. Stuber, *Orthogonal Frequency Division Multiplexing for Wireless Communications*. Springer Science & Business Media, 2006.
- [30] H. Bolcskei, M. Borgmann, and A. J. Paulraj, "Impact of the propagation environment on the performance of space-frequency coded mimo-ofdm," *IEEE J. Sel. Areas Commun.*, vol. 21, no. 3, pp. 427–439, 2003.
- [31] M. Park, H. Jun, J. Cho, N. Cho, D. Hong, and C. Kang, "Papr reduction in ofdm transmission using hadamard transform," in *Proc. IEEE Int. Conf. Commun. (ICC)*, 2000, pp. 430–433.

- [32] Y. Shao and D. Gunduz, "Semantic communications with discrete-time analog transmission: A papr perspective," *IEEE Wireless Commun. Lett.*, vol. 12, no. 3, pp. 510–514, 2022.
- [33] P. Hu, J. Im, Z. Asgar, and S. Katti, "Starfish: Resilient image compression for aiot cameras," in *Proc. ACM Conf. Embed. Netw. Sensor Syst. (SenSys)*, 2020, pp. 395–408.
- [34] R. Wang, H. Liu, J. Qiu, M. Xu, R. Guérin, and C. Lu, "Progressive neural compression for adaptive image offloading under timing constraints," in *Proc. IEEE Real-Time Syst. Symp. (RTSS)*, 2023, pp. 118–130.
- [35] Y. Cheng, Z. Zhang, H. Li, A. Arapin, Y. Zhang, Q. Zhang, Y. Liu, K. Du, X. Zhang, F. Y. Yan et al., "GRACE: Loss-Resilient Real-Time video through neural codecs," in *Proc. USENIX NSDI*, 2024, pp. 509–531.
- [36] Z. He, Y. Yang, L. Qiu, K. Park, and Y. Yang, "Nerve: Real-time neural video recovery and enhancement on mobile devices," *Proc. ACM Conf. Emerg. Netw. Exper. Technol. (CoNEXT)*, vol. 2, no. 4, pp. 1–19, 2024.
- [37] D. B. Kurka and D. Gündüz, "Bandwidth-agile image transmission with deep joint source-channel coding," *IEEE Trans. Wireless Commun.*, vol. 20, no. 12, pp. 8081–8095, 2021.
- [38] G. Zhang, Q. Hu, Z. Qin, Y. Cai, G. Yu, and X. Tao, "A unified multi-task semantic communication system for multimodal data," *IEEE Trans. Commun.*, vol. 72, no. 7, pp. 4101–4116, 2024.
- [39] T.-Y. Tung, D. B. Kurka, M. Jankowski, and D. Gündüz, "Deepjscc-q: Constellation constrained deep joint source-channel coding," *IEEE J. Sel. Areas Inf. Theory*, vol. 3, no. 4, pp. 720–731, 2022.
- [40] M. Liu, W. Chen, J. Xu, and B. Ai, "Real-time implementation and evaluation of sdr-based deep joint source-channel coding," in *Proc. IEEE Veh. Technol. Conf. (VTC)*. IEEE, 2022, pp. 1–5.
- [41] Y. Wang, M. Chen, T. Luo, W. Saad, D. Niyato, H. V. Poor, and S. Cui, "Performance optimization for semantic communications: An attention-based reinforcement learning approach," *IEEE J. Sel. Areas Commun.*, vol. 40, no. 9, pp. 2598–2613, 2022.
- [42] H. Du, J. Wang, D. Niyato, J. Kang, Z. Xiong, and D. I. Kim, "Ai-generated incentive mechanism and full-duplex semantic communications for information sharing," *IEEE J. Sel. Areas Commun.*, vol. 41, no. 9, pp. 2981–2997, 2023.
- [43] C. Liu, C. Guo, Y. Yang, W. Ni, and T. Q. Quek, "Ofdm-based digital semantic communication with importance awareness," *IEEE Trans. Commun.*, 2024.
- [44] J. Terry and J. Heiskala, *OFDM Wireless LANs: A Theoretical and Practical Guide*. Sams publishing, 2002.
- [45] W. Zhang, H. Zhang, H. Ma, H. Shao, N. Wang, and V. C. Leung, "Predictive and adaptive deep coding for wireless image transmission in semantic communication," *IEEE Trans. Wireless Commun.*, vol. 22, no. 8, pp. 5486–5501, 2023.
- [46] B. Hanin, "Which neural net architectures give rise to exploding and vanishing gradients?" in *Adv. Neural Inf. Process. Syst. (NeurIPS)*, 2018, pp. 1–10.
- [47] D. Tse and P. Viswanath, *Fundamentals of Wireless Communication*. Cambridge university press, 2005.
- [48] 3rd Generation Partnership Project (3GPP), "Study on channel model for frequencies from 0.5 to 100 ghz (release 14)," 3GPP, Tech. Rep. 3GPP TR 38.901, 2017, online; accessed: 16 February 2025. [Online]. Available: https://www.3gpp.org/ftp/Specs/archive/38_series/38.901/38901-100.zip
- [49] J. C. Bezdek and R. J. Hathaway, "Convergence of alternating optimization," *Neural, Parallel & Scientific Computations*, vol. 11, no. 4, pp. 351–368, 2003.
- [50] CVX Research, "CVX: Matlab Software for Disciplined Convex Programming," <https://cvxr.com/cvx/>, 2025, online; accessed: 16 February 2025.
- [51] K. He, X. Zhang, S. Ren, and J. Sun, "Deep residual learning for image recognition," in *Proc. IEEE/CVF Conf. Comput. Vis. Pattern Recognit. (CVPR)*, 2016, pp. 770–778.
- [52] K. Soomro, A. R. Zamir, and M. Shah, "Ucf101: A dataset of 101 human actions classes from videos in the wild," *arXiv preprint arXiv:1212.0402*, 2012.
- [53] J. Li, B. Li, and Y. Lu, "Deep contextual video compression," in *Adv. Neural Inf. Process. Syst. (NeurIPS)*, 2021, pp. 18 114–18 125.
- [54] Ettus Research, "USRP X300/X310," <https://kb.ettus.com/X300/X310>, 2025, online; accessed: 16 February 2025.
- [55] —, "USRP Hardware Driver and USRP Manual," <https://files.ettus.com/manual/>, 2025, online; accessed: 16 February 2025.
- [56] B. P. Crow, I. Widjaja, J. G. Kim, and P. T. Sakai, "Ieee 802.11 wireless local area networks," *IEEE Commun. Mag.*, vol. 35, no. 9, pp. 116–126, 1997.
- [57] R. Gallager, "Low-density parity-check codes," *IEEE Trans. Inf. Theory*, vol. 8, no. 1, pp. 21–28, 1962.
- [58] J. Deng, W. Dong, R. Socher, L.-J. Li, K. Li, and L. Fei-Fei, "Imagenet: A large-scale hierarchical image database," in *Proc. IEEE/CVF Conf. Comput. Vis. Pattern Recognit. (CVPR)*, 2009, pp. 248–255.
- [59] Rich Franzen, "Kodak Lossless True Color Image Suite," <https://r0k.us/graphics/kodak/>, 2025, online; accessed: 10 February 2025.
- [60] T. Xue, B. Chen, J. Wu, D. Wei, and W. T. Freeman, "Video enhancement with task-oriented flow," *Int. J. Comput. Vis.*, vol. 127, pp. 1106–1125, 2019.
- [61] G. J. Sullivan, J.-R. Ohm, W.-J. Han, and T. Wiegand, "Overview of the high efficiency video coding (hevc) standard," *IEEE Trans. Circuits Syst. Video Technol.*, vol. 22, no. 12, pp. 1649–1668, 2012.
- [62] L. Guo, W. Chen, Y. Sun, B. Ai, N. Pappas, and T. Quek, "Diffusion-driven semantic communication for generative models with bandwidth constraints," *IEEE Trans. Wireless Commun.*, 2025.
- [63] S. Fouladi, J. Emmons, E. Orbay, C. Wu, R. S. Wahby, and K. Winstein, "Salsify: Low-latency network video through tighter integration between a video codec and a transport protocol," in *Proc. USENIX NSDI*, 2018, pp. 267–282.
- [64] C. Bian, Y. Shao, H. Wu, E. Ozfatura, and D. Gündüz, "Process-and-forward: Deep joint source-channel coding over cooperative relay networks," *IEEE J. Sel. Areas Commun.*, 2025.